nanomaterials

MDPI

Article

Experimental and Computational Analysis of MnO_2@V_2C-MXene for Enhanced Energy Storage

Mahjabeen Fatima [1], Syedah Afsheen Zahra [1], Saleem Ayaz Khan [2,*], Deji Akinwande [3], Jan Minár [2] and Syed Rizwan [1,*]

[1] Physics Characterization and Simulations Lab (PCSL), Department of Physics, School of Natural Sciences (SNS), National University of Sciences and Technology (NUST), Islamabad 44000, Pakistan; mahjabeen.fatima96@gmail.com (M.F.); afsheenzahra@outlook.com (S.A.Z.)
[2] New Technologies Research Centre, University of West Bohemia, Univerzitni 2732, 306 14 Pilsen, Czech Republic; jmminar@gmail.com
[3] Microelectronics Research Centre, The University of Texas at Austin, Austin, TX 78758, USA; deji@ece.utexas.edu
* Correspondence: khan@kmm.zcu.cz (S.A.K.); syedrizwan@sns.nust.edu.pk (S.R.)

Abstract: Herein, we studied the novel and emerging group of 2D materials namely MXene along with its nanocomposites. This work entails detailed experimental as well as computational study of the electrochemical behavior of vanadium carbide (V_2CT_x) MXene and MnO_2-V_2C nanocomposite with varying percentages of MnO_2. A specific capacitance of 551.8 F/g was achieved for MnO_2-V_2C nanocomposite in 1 M KOH electrolyte solution, which is more than two times higher than the gravimetric capacitance of 196.5 F/g obtained for V_2C. The cyclic stability achieved for the MnO_2-V_2C nanocomposite resulted in a retentivity of 96.5% until 5000 cycles. The c-lattice parameter achieved for MXene is 22.6 Å, which was 13.01 Å for MAX phase. The nanocomposite resulted in a c-lattice parameter of 27.2 Å, which showed that the spatial distance between the MXene layers was efficiently obtained. The method of wet etching was used for the preparation of pristine MXene and the liquid phase precipitation method was opted for the synthesis of the MnO_2-V_2C nanocomposite. Density functional theory calculation was exercised so as to complement the experimental results and to understand the microscopic details, such as structure stability and electronic structure. The current report presents a comprehensive experimental and computational study on 2D MXenes for future energy storage applications.

Keywords: V_2C MXene; energy storage; supercapacitors; two-dimensional materials; density functional theory

Citation: Fatima, M.; Zahra, S.A.; Khan, S.A.; Akinwande, D.; Minár, J.; Rizwan, S. Experimental and Computational Analysis of MnO_2@V_2C-MXene for Enhanced Energy Storage. *Nanomaterials* **2021**, *11*, 1707. https://doi.org/10.3390/nano11071707

Academic Editor: Liang Huang

Received: 26 March 2021
Accepted: 21 April 2021
Published: 29 June 2021

1. Introduction

Two-dimensional (2D) materials involve uncommon and rare electronic, mechanical as well as optical properties [1–5], that have led to its wide-ranging analysis for versatile applications in the past decade. In addition, they aid to an expedient building block for diverse layered structures, membranes and composites [6–10]. MXenes—the fresh and newest accoutrement to the world of 2D materials—are basically early transition metal carbides, nitrides and carbonitrides [11–15]. Generally, the formula for MXenes is $M_{n+1}X_nT_x$ (n = 1 to 3), whereas M symbolizes an earlier transition metal (Ti, Nb, Ta, Mo, V), X is carbon and/or nitrogen and T_x denotes the surface terminations (hydroxyl, oxygen or fluorine) [16]. Examples may include V_2CT_x [17], $Ti_3C_2T_x$ [18] and $Nb_4C_3T_x$ [15]. MXenes involve (n + 1) M layers that are enfolded 'n' layers of X in an $[MX]_nM$ sequence. MXenes are obtained from selective etching of 'A' layers from their lamellar precursors, known as MAX. MXenes are a huge class of ternary carbides and nitrides, including more than 70 reported phases until now, along with various solid solutions and ordered double transition metal structures [19–25].

Vahid et al. studied electrical and optical properties of two-dimensional V_2C, revealing intriguing possibilities and opening the door for versatile energy storage applications [26]. Yoon et al. reported delaminated V_2C MXene with phosphorus obtained from triphenylphosphine intercalated in sheets, for activation of hydrogen evolution reactions from a non-metallic electron donor [27]. Shan et al. recently reported V_2C MXene as an efficient electrode in various aqueous electrolytes for supercapacitor applications, revealing a different energy density and the highest power density of the V_2C electrode in several electrolytes [28]. The theoretical insights of V_2C have also been studied, which reveal it is a capable anode material for lithium-ion batteries and shows a theoretical storage capacity of 940 mAh/g [29–32].

This article elaborates on the experimental and computational details and insights of pristine V_2C and the MnO_2-V_2C nanocomposite. It observes the trends of vanadium-based MXene when MnO_2 is adsorbed on the pristine MXene and analyzes the density of states and bandgap via density functional theory [33–35], for suitability in energy storage applications.

2. Experimental Methods

Figure 1a shows an XRD of selective etching of Al layer from V_2AlC to obtain V_2CT_x. One gram of V_2AlC MAX (300 mesh) was treated with 49% concentrated hydrofluoric acid for various time periods at room-temperature from which wet-etching for 116 h showed favorable results. The etched sample was washed via centrifugation and vacuum filtration with a powdered sample of V_2C. However, Pristine V_2C cannot exist due to its high surface reactivity and readily oxidizes at ambient temperatures. Therefore, MXene with surface terminations was obtained after drying in a vacuum oven for 24 h. The MnO_2-V_2CT_x nanocomposite was synthesized by the liquid-phase precipitation method. Two hundred milligrams of V_2CT_x powder was dispersed in 100 mL of a 1 mM aqueous solution of MnO_2 with constant magnetic stirring at 40 °C for a time period of 6 h. A precipitate was collected by centrifugation and rinsing with ethanol and DI water separately three times with the help of vacuum filtration. The powder obtained was then dried out in the vacuum oven at 55 °C for 24 h. With this method, five different samples of varying percentages, namely 10%, 20%, 30%, 40% and 50%, were synthesized as the amount of MnO_2 was increased.

3. Results and Discussion

The XRD patterns of the MAX phase and MXene etched with 49% HF solution for different times and divulging structural evolution are shown. The sharp peaks at 2Θ= 13.28°, 41.09° and 55.7° of the MAX precursors represents its high crystallinity and purity. Exposure to HF results in shifting of the (002) peak in the XRD pattern of V_2AlC to a lower angle, indicating the increased interlayer spacing of synthesized V_2CT_x MXene (JCPD 03-065-2628). The sample etched for 116 h shows the strongest intensity and the lowest angle of (002) diffraction peaks at 2Θ= 7.4°. The shifting of the peak is the result of an increased c-lattice that is 22.6 Å instead of 13.01 Å for pristine MAX. Small peaks of MAX phase in MXene represent the unetched MXene as suggested by previous studies [36–39]. The peak at 55.7° persists in MXene due to the presence of traces of MAX in MXene. Additionally, there is a small peak at 57.6° which indicates the presence of V_2C. Further increase in etching time results in decreased intensity and shifting of the (002) diffraction peak towards a larger angle due to the dissolved V_2C sheets. The XRD patterns of nanocomposite samples shown in Figure 1b confirm the presence of MnO_2 along with V_2CT_x. The broadening of the (002) diffraction peak and the shift towards a lower angle suggests that there is increased interlayer spacing of composite material. The presence of additional broad peaks of the MnO_2-V_2CT_x nanocomposite material at a 2Θvalue of 35.5° and 39.6° are ascribed to the (112) and (101) planes of polycrystalline orthorhombic MnO_2 (JCPD 00-0300820) [40]. This broadening of peaks is a result of reduced crystallinity of MnO_2 over V_2CT_x sheets. A small peak of V_2O_5 near a 2Θvalue of 42.7° can be observed, which is produced as a result of heat produced during the etching process [41]. Vanishing of the (002) diffraction

peak with the increased weight percent of MnO_2 is a result of decreased crystallinity of the MnO_2-V_2CT_x nanocomposites.

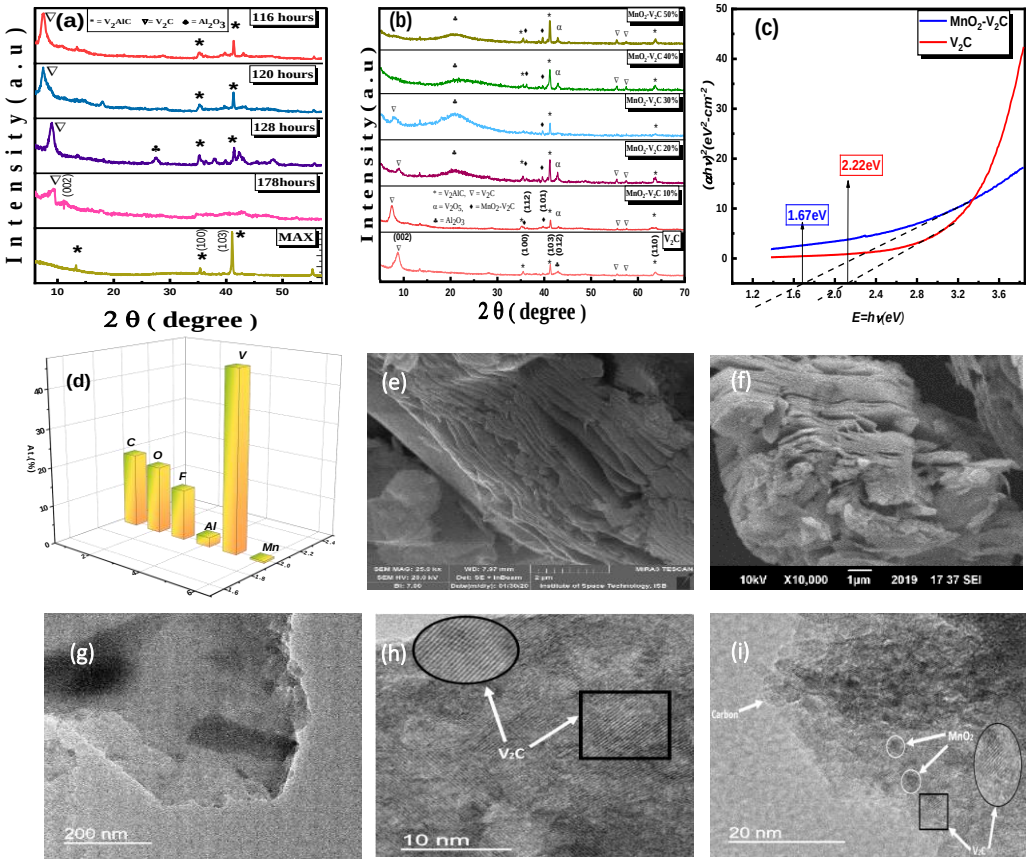

Figure 1. (**a**) XRD of pristine V_2AlC and prepared V_2CT_x etched for varying time periods, (**b**) XRD of V_2C MXene nanocomposites with varying weight percentages of MnO_2, (**c**) bandgap analysis of V_2C and MnO_2-V_2C nanocomposite, (**d**) EDX for the elemental analysis of MnO_2-V_2C nanocomposite, (**e**) micrograph for pristine V_2C, (**f**) micrograph for MnO_2-V_2C nanocomposite. (**g**) TEM image of V_2C at 200 nm, (**h**) TEM image of V_2C at 10 nm, (**i**) TEM image of MnO_2-V_2C nanocomposite.

The bandgaps of pristine V_2C and MnO_2-V_2C samples in Figure 1c depict that, similar to pristine MXene, the MnO_2-V_2C nanocomposite has shown a direct optical bandgap. The values of energy gained after calculations reveal that pristine V_2C had a bandgap of 2.22 eV and was reduced to 1.67 eV after the formation of the nanocomposite. The decrease in bandgap is observed upon intercalation of MnO_2 due to the Mn bonding with the termination sites of V_2C. The MXene in general are covered with the termination sites that may include -H -O, -F, -OH and -OF [42]. Mn bond with the termination sites of V_2C thus lead to the creation of defects in the layered MXene. Figure 1d shows the elemental analysis of the MnO_2-V_2C nanocomposite. Furthermore, the images obtained from the scanning electron microscope (SEM) in Figure 1e show the layered structure of V_2C obtained after HF treatment of MAX phase resulting in fanning out and spreading of basal planes, which is a clear indication of a successful etching process. The layered structure in Figure 1f persists even in 10% MnO_2-V_2C sample which signifies that the structure of V_2C has not been destroyed during the formation of the nanocomposite. Figure 1g reveals the TEM image of V_2C at 200 nm which, when further magnified, clearly shows the layered structure of pristine MXene as in Figure 1h. Moreover, the presence of a whitish carbon layer is observed in Figure 1i, whereas the dark patch is clearly seen over V_2C sheets in Figure 1i, indicating the presence of MnO_2; Tang et al. report MnO_2-Ti_3C_2 nanocomposite which

reveals a dark patchy structure formed by MnO_2 over Ti_3C_2 sheets [39], similar to that of the MnO_2-V_2C nanocomposite.

In Figure 2, a peak is observed at 394 cm^{-1}, which is the characteristic peak for Al-V vibrations [43], that confirms the presence of V_2AlC, whereas several broad peaks arise in the MXene phase at 657 cm^{-1}, 1339 cm^{-1}, 1704 cm^{-1}, and 2143 cm^{-1} which contribute to V-C vibrations [44]. Along with the peaks of V-C, vibrational peaks of Al-V have also been observed in the nanocomposite samples. This occurs because of the presence of a little amount of MAX phase even after etching. The intensity of modes was enhanced in the MnO_2-V_2C nanocomposite when MnO_2 percentage is increased, compared to pristine V_2C. In 10% MnO_2-V_2C nanocomposite, the peak is much broader compared to 20%, 30% and 40%. This might occur due to the enhancement of motions of atoms after the formation of the nanocomposite. The peaks of MnO_2 arise around 200 cm^{-1} and 500–600 cm^{-1} [45] while for pristine V_2C, the peaks arise around 600–2100 cm^{-1}. As previously discussed regarding graphene as a parental family to MXenes, Chen et al. reports an MnO_2/Graphene-Oxide nanocomposite peak around 1750 cm^{-1} [46], which is close enough to vary from the percentage of the MnO_2-V_2C nanocomposite peak that is around 1767 cm^{-1}. Moreover, for the pristine V_2C optical modes, the foremost three optical branches in phonon spectrum show considerably lesser frequencies and are near to three acoustic phonon branches, which results in a phonon gap among the lower three and upper three optical branches. This is one of the typical properties of MXene, which is observed in numerous MXene families [47]. Furthermore, substantial contribution comes from vibrations of V-atoms. It can be observed that the motion of V-atoms is weakened by vibrations of the terminal atoms, which concludes a noticeable difference between pristine V_2C system and V_2CT_x. Since no robust signal of vanadium oxide was detected in MnO_2-V_2C samples, this shows that either the V_2CT_x sheets are not oxidized, or limited MXene flakes are oxidized beyond the detection of Raman technique, indicating the low density of vanadium oxide on the surface of V_2CT_x. The remaining peaks shown in the varying percentage samples are of Al-V vibrations, as a little amount of aluminum persists in the pristine MXene sample. Moreover, Figure S1 in Supplementary Materials discussed the FTIR graphs for pristine V_2C MXene and (10%, 20%, 30% 40%, 50% weight) MnO_2-V_2C nanocomposites. The peaks fairly signify the MXene formation and presence of MnO_2 peaks in MXene plots.

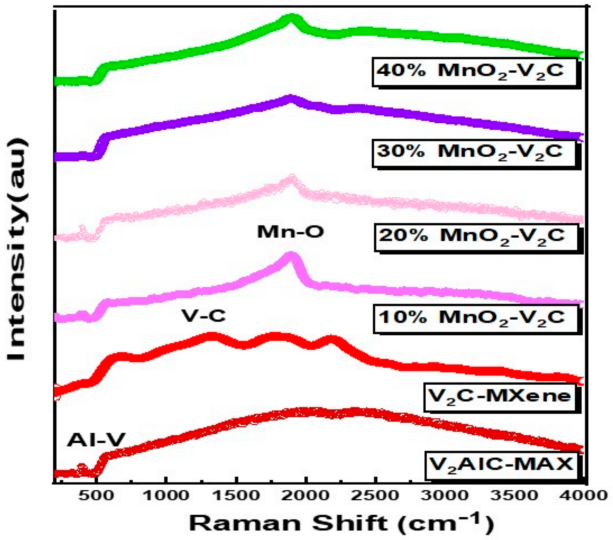

Figure 2. Raman spectroscopy for V_2AlC, pristine V_2C and MnO_2-V_2C nanocomposite at varying percentages.

Computational Framework: The computational analysis was carried out with the help of the ab initio all-electron FLAPW method, as executed in the WIEN2k code [33,34]. The calculations were performed using Perdew–Burke–Ernzerhof (PBE) generalized gradient

approximation (GGA) exchange-correlation functional [35,48,49]. Ground state structure for V_2C MXene was attained by relaxation of internal coordinates. Furthermore, the density of states (DOS), band structure, and electronic density was calculated for the relaxed structure using GGA. For a clear description of the experimental observations and to the point information about the structure, the c-lattice parameter was increased up to 22.6 Å. Consequently, the V_2C MXene nanocomposite relaxed structure had to be generated, for which we used GGA-PBE with 64 k-points in the irreducible Brillouin zone (IBZ). DOS along with the band structure was calculated and analyzed for doped and adsorbed Mn atom on MXene. Wave function in the interstitial regions was expanded in plane waves, with the plane wave cut-off chosen as $R_{MT}K_{max}$ = 7.0. R_{MT} represents the smallest radius of the atomic sphere and K_{max} as the largest wave-vector magnitude. The R_{MT} were taken as 1.86 a.u. for V-atoms, 1.55 a.u. for O-atoms, 1.68 a.u. for F-atoms, 1.63 a.u. for C-atoms and 1.80 a.u. for Mn-atom. The K points for structure relaxation is 2 k-points in irreducible Brillouin zone (IBZ) with k-grid of 2 × 2 × 1. In addition to that, k-points for energy convergence are 54 k points in IBZ with k grid of 6 × 6 × 3. Moreover, the forces relaxation criteria were kept at 10^{-4} Ryd and energy convergence criteria was fixed at 10^{-5} Ryd.

The system of V_2C-OF is modelled by a supercell of slabs. Bowman et al. explains the crystal structure of V_2C [50]. Ideally, simple V_2C structure could have been considered but herein we inculcated V_2C along with its surface terminations in order to complement the experimental analysis, because pristine V_2C cannot exist in ordinary atmospheric conditions. The carbon atom is sandwiched between vanadium layers. The oxygen and fluorine atomic layers were added to the system as functional terminations on to the surface, as shown in Figure 3a. A supercell of 2 × 2 × 1 was initially constructed to examine the stability of manganese in slab using different positions of the Mn atom. For obtaining a stable position of the Mn atom in the V_2C-OF system, we constructed two different configurations that are by adsorption of the Mn atom and by doping of the Mn atom in the V_2C-OF system, as shown in Figure 3b,c respectively. The electronic structure of Mn-adsorbed atom was then studied using 4 × 4 × 1 supercell as in Figure 3d.

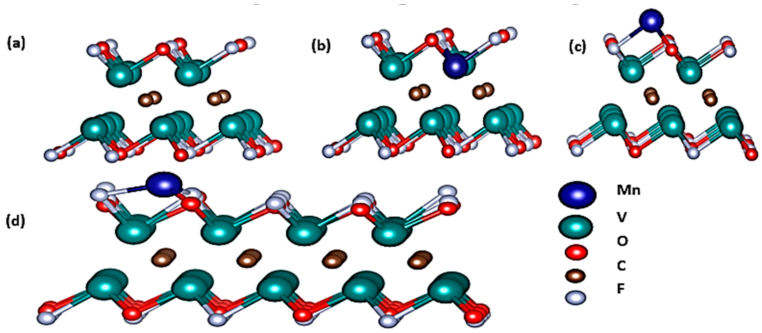

Figure 3. (**a**) Structure of pristine V_2C, (**b**) structure of Mn-doped V_2C, (**c**) structure of Mn-adsorbed V_2C in 2 × 2 × 1 supercell, (**d**) structure of Mn-adsorbed V_2C in 4 × 4 × 1 supercell.

The electronic structure of the Mn-adsorbed atom was then studied using 4 × 4 × 1 supercell. In the Mn-adsorbed structure, the Mn atom forms a bond with the termination sites, i.e., O and F, while in a doped structure, the Mn-atom substitutes the V-atom. Figure 4a illustrates the density of states (DOS) vs. energy plots for V_2C-OF and Mn-adsorbed V_2C-OF. Figure 4a clearly shows that the density of states has been drastically increased in the conduction band around 0 to 2 eV for Mn-adsorbed V_2C-OF structure as compared to a simple V_2C-OF system. The increase in major peaks of V in the conduction band is because of the presence of Mn-adsorption sites which are nearer to the V-atomic sites.

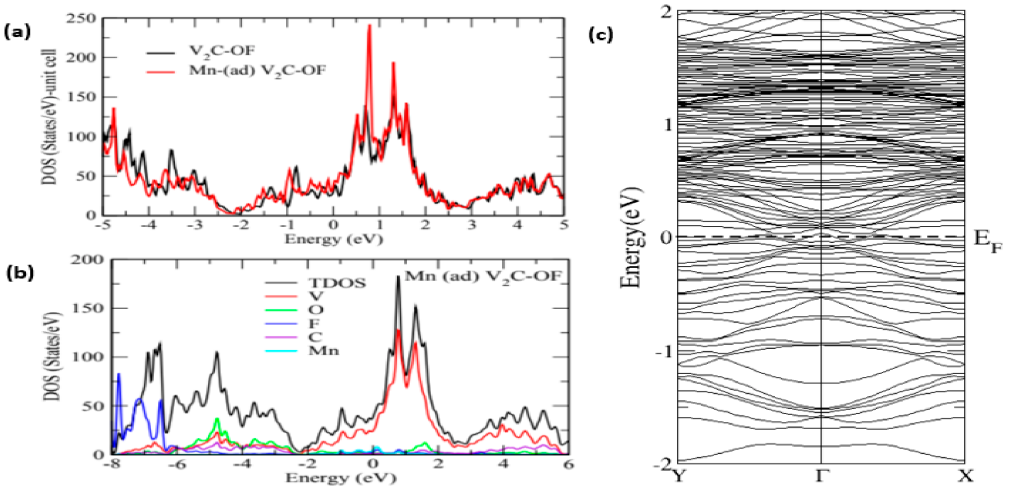

Figure 4. (**a**) DOS vs. energy V_2C-OF and Mn-adsorbed V_2C-OF, (**b**) total DOS vs. energy V_2C-OF and Mn-adsorbed V_2C-OF, (**c**) electronic bandgap structure for Mn-adsorbed V_2C-OF.

From Figure 4b, it is seen that Mn peaks are existing in the conduction band around 0–1 eV and are contributing to the total density of states (TDOS) which is the reason for an increase in the density of states. Moreover, Figure 4c shows the bandgap structure for Mn-adsorbed V_2C-OF that shows complete metallic behavior, since the bandgap theoretically obtained for pristine MXene is zero [51–53]. The experimentally obtained bandgap, however, is found to be different from the one theoretically explained. Since the experimentally obtained data of the bandgap structure has shown a decrease in bandgap, it thus concludes the enhancement in the electronic properties of V_2C structure.

Electrochemical Analysis: The cyclic voltammetry (CV) reveals the I-V curves of pristine V_2C and the MnO_2-V_2C nanocomposite, which was discerned at a potential window of 0.0 V to +0.9 V while the scan rate was fixed as 100 mV/s. V_2C however oxidizes rapidly due to its surface reactivity [54,55] but the oxidized samples can be investigated by storing diluted samples of V_2C in sealed Eppendorf vials at room temperature and analyzing the samples first. Furthermore, MnO_2 adsorption in V_2C helps in omitting unwanted surface attachments. Figure 5a shows the current vs. voltage graph, which reveals that the gravimetric capacitance for V_2C is about 196.5 F/g, larger than the value reported in [29], and the highest gravimetric capacitance obtained for the MnO_2-V_2C nanocomposite is about 551.8 F/g. The enhanced value of gravimetric capacitance of the MnO_2-V_2C nanocomposite is more than twice that obtained for pristine MXene.

MnO_2-V_2C nanocomposite exhibited high values of specific capacitance compared to pristine V_2C. It is encompassing all other factors, i.e., a high specific area and increased storage ability, due to its morphology which is generally a flake-like structure. At comparably higher current density, K^+ ions are diffused from the 1 M KOH electrolyte into the nanocomposite and gain access i.e., they penetrate into the gaps available between nanocomposite layers easily, which leads to an efficient charge–discharge ratio [56]. Until 5000 cycles, the results are excellent as the 5000th cycle's gravimetric capacitance obtained was 532.6 F/g. The reason for decreased efficiency is the degradation of electrode material, though it signifies that retentivity is very high, at about 96.5% of the original value. Figure 5b shows a comparison of the nanocomposite's 1st cycle and 5000th cycle curve, which reveals that theoretical study has complemented the experimental data. The theoretical results stated that with the enhancement of electronic density and the stability of adsorbed Mn-atom in MXene, which is fairly seen by the comparison graph of current-voltage cycles, a high specific capacitance has been achieved after Mn adsorption with viable stability up to 5000 cycles. Bare V_2C cannot show such a high specific capacitance due to hydrophilicity and thus readily oxidizes in the atmosphere. Figure 5d adds to the argument of cyclic stability of the nanocomposite, which also reveals that a very high retentivity percentage

of specific capacitance has been achieved, even after 5000 cycles. Moreover, the obtained galvanostatic charge–discharge triangular curves for pristine V_2C and MnO_2-V_2C can be seen in Figure 5c, revealing an outstanding and improved performance of the nanocomposite electrode material, as it is providing a high gravimetric capacitance even after a longer time period.

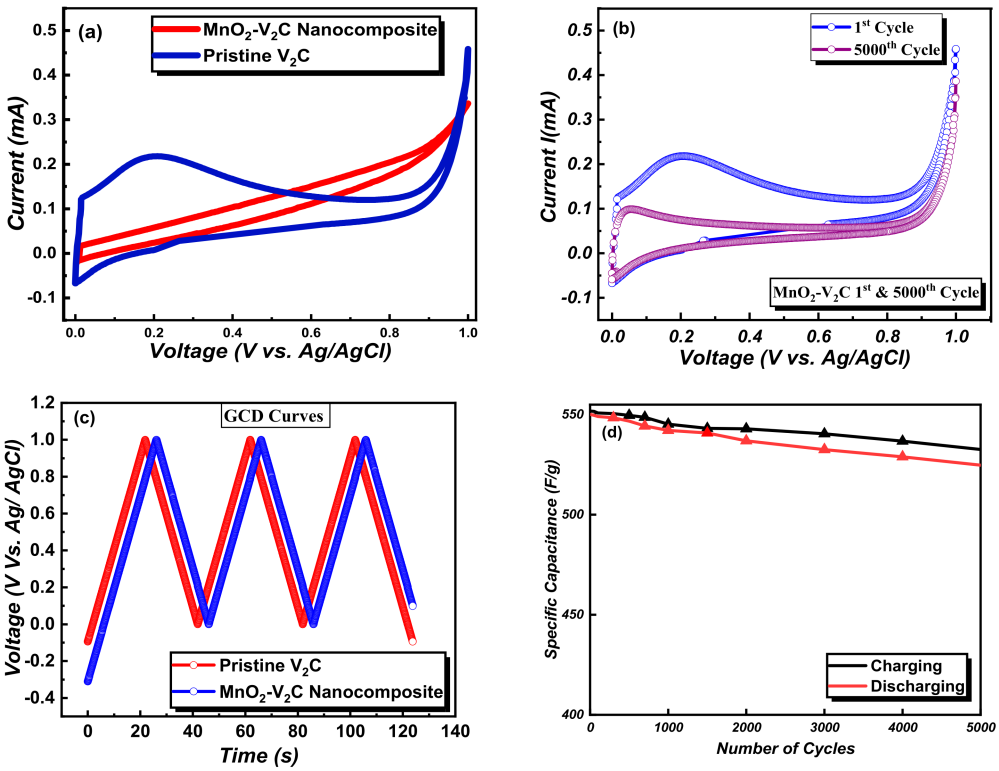

Figure 5. (**a**) Current vs. voltage of pristine MXene and MnO_2-V_2C nanocomposite, (**b**) comparison of 1st and 5000th cycle of MnO_2-V_2C nanocomposite, (**c**) galvanostatic charge–discharge curves of V_2C and MnO_2-V_2C, (**d**) specific capacitance vs. number of cycles.

4. Conclusions

The two-dimensional materials with the general formula V_2CT_x were synthesized after wet-chemical etching from the bulk parent compound MAX. This article reported experimental as well as theoretical outcomes on structural, morphological and optoelectronic properties of pristine MXene and MnO_2-MXene nanocomposites. XRD revealed that the c-lattice parameter increased from 13.01 Å to 22.6 Å for MAX and MXene respectively, and then reached 27.2 Å for the MnO_2-V_2C nanocomposite, signifying adsorption-dominant properties. SEM, EDX, and bandgap analysis demonstrated that the adsorption of MnO_2 in V_2C, which showed an intriguing gravimetric capacitance in the MnO_2-MXene nanocomposite of approximately 551.8 F/g, has a retentivity of about 96.5% after 5000 cycles. The computational analysis supported the experimental data as the density of states inevitably increased when MnO_2 was adsorbed in V_2C.

Supplementary Materials: The following are available online at https://www.mdpi.com/article/10.3390/nano11071707/s1, Figure S1 in Supplementary Materials discussed the FTIR graphs for pristine V_2C MXene and (10%, 20%, 30% 40%, 50% weight) MnO_2-V_2C nanocomposites. The peaks fairly signify the MXene formation and presence of MnO_2 peaks in MXene plots.

Author Contributions: M.F. and S.A.Z. has analyzed experimental data and has written the manuscript. S.A.K. and J.M. has extensively helped in computational analysis. D.A. helped in analysis of the experimental results. S.R. conceived the research concept, wrote the manuscript and supervised the complete project. All authors have read and agreed to the published version of the manuscript.

Funding: This research received funding from the United States Agency for International Development (USAID) and the Higher Education Commission (HEC) of Pakistan under the Project No.: HEC/R&D/PAKUS/2017/783. Also, partial funding was received from Computational and Experimental Design of Advanced Materials with New Functionalities (CEDAMNF; grant CZ.02.1.01/0.0/0.0/15_003/0000358) of the Ministry of Education, Youth and Sports (Czech Republic) and GAČR (Proj. 20-18725S).

Data Availability Statement: The data supporting the findings of "Experimental and Computational Analysis of MnO_2@V_2C-MXene for Enhanced Energy Storage" are available within the manuscript and the corresponding supporting information file.

Acknowledgments: The authors are thankful to the United States government and its people, the United States Agency for International Development (USAID) and the Higher Education Commission (HEC) of Pakistan for providing research funding under the Project No.: HEC/R&D/PAKUS/2017/783. Saleem Ayaz Khan is grateful for support from Computational and Experimental Design of Advanced Materials with New Functionalities (CEDAMNF; grant CZ.02.1.01/0.0/0.0/15_003/0000358) of the Ministry of Education, Youth and Sports (Czech Republic) and GAČR (Proj. 20-18725S).

Conflicts of Interest: The authors declare no conflict of interest.

References

1. Fiori, G.; Bonaccorso, F.; Iannaccone, G.; Palacios, T.; Neumaier, D.; Seabaugh, A.; Banerjee, S.K.; Colombo, L. Electronics based on two-dimensional materials. *Nat. Nanotechnol.* **2014**, *9*, 768–779. [CrossRef] [PubMed]
2. Nicolosi, V.; Chhowalla, M.; Kanatzidis, M.G.; Strano, M.S.; Coleman, J.N. Liquid exfoliation of layered materials. *Science* **2013**, *340*, 6139. [CrossRef]
3. Xia, F.; Wang, H.; Di, X.; Dubey, M.; Ramasubramaniam, A. Two-dimensional material nanophotonics. *Nat. Photonics* **2014**, *8*, 899–907. [CrossRef]
4. Akinwande, D.; Petrone, N.; Hone, J. Two-dimensional flexible nanoelectronics. *Nat. Commun.* **2014**, *5*, 1–12. [CrossRef] [PubMed]
5. Cepellotti, A.; Fugallo, G.; Paulatto, L.; Lazzeri, M.; Mauri, F.; Marzari, N. Phonon hydrodynamics in two-dimensional materials. *Nat. Commun.* **2015**, *6*, 1–7. [CrossRef] [PubMed]
6. Geim, A.K.; Grigorieva, I.V. Van der Waals heterostructures. *Nature* **2013**, *499*, 419–425. [CrossRef]
7. Cahangirov, S.; Topsakal, M.; Aktürk, E.; Şahin, H.; Ciraci, S. Two-and one-dimensional honeycomb structures of silicon and germanium. *Phys. Rev. Lett.* **2009**, *102*, 236804. [CrossRef]
8. Lalmi, B.; Oughaddou, H.; Enriquez, H.; Kara, A.; Vizzini, S.; Ealet, B.; Aufray, B. Epitaxial growth of a silicene sheet. *Appl. Phys. Lett.* **2010**, *97*, 223109. [CrossRef]
9. Nowak, I.; Ziolek, M. Niobium compounds: Preparation, characterization, and application in heterogeneous catalysis. *Chem. Rev.* **1999**, *99*, 3603–3624. [CrossRef]
10. Asghar, M.; Zahra, S.A.; Khan, Z.; Ahmed, M.; Nasir, F.; Iqbal, M.; Mohammad, M.A.; Mahmood, A.; Akinwande, D.; Rizwan, S. Laser-Assisted Fabrication of Nanostructured Substrate Supported Electrodes for Highly Active Supercapacitors. *Front. Mater.* **2020**, *7*, 179. [CrossRef]
11. Naguib, M.; Kurtoglu, M.; Presser, V.; Lu, J.; Niu, J.; Heon, M.; Hultman, L.; Gogotsi, Y.; Barsoum, M.W. Two-dimensional nanocrystals produced by exfoliation of Ti_3AlC_2. *Adv. Mater.* **2011**, *23*, 4248–4253. [CrossRef]
12. Naguib, M.; Mashtalir, O.; Carle, J.; Presser, V.; Lu, J.; Hultman, L.; Gogotsi, Y.; Barsoum, M.W. Two-dimensional transition metal carbides. *ACS Nano* **2012**, *6*, 1322–1331. [CrossRef]
13. Naguib, M. Multifunctional Pure MXene Fiber from Liquid Crystals of Only Water and MXene. *ACS Cent. Sci.* **2020**, *6*, 344–346. [CrossRef]
14. Khazaei, M.; Arai, M.; Sasaki, T.; Chung, C.-Y.; Venkataramanan, N.S.; Estili, M.; Sakka, Y.; Kawazoe, Y. Novel electronic and magnetic properties of two-dimensional transition metal carbides and nitrides. *Adv. Funct. Mater.* **2013**, *23*, 2185–2192. [CrossRef]
15. Ghidiu, M.; Naguib, M.; Shi, C.; Mashtalir, O.; Pan, L.M.; Zhang, B.; Yang, J.; Gogotsi, Y.; Billinge, S.J.L.; Barsoum, M.W. Synthesis and characterization of two-dimensional Nb_4C_3 (MXene). *Chem. Commun.* **2014**, *50*, 9517–9520. [CrossRef]
16. Mei, J.; Ayoko, G.A.; Hu, C.; Bell, J.M.; Sun, Z. Two-dimensional fluorine-free mesoporous Mo_2C MXene via UV-induced selective etching of Mo_2Ga_2C for energy storage. *Sustain. Mater. Technol.* **2020**, *25*, e00156. [CrossRef]
17. Wu, M.; Wang, B.; Hu, Q.; Wang, L.; Zhou, A. The synthesis process and thermal stability of V2C MXene. *Materials* **2018**, *11*, 2112. [CrossRef]
18. Gao, Q.; Sun, W.; Ilani-Kashkouli, P.; Tselev, A.; Kent, P.R.; Kabengi, N.; Naguib, M.; Alhabeb, M.; Tsai, W.Y.; Baddorf, A.P.; et al. Tracking ion intercalation into layered Ti_3C_2 MXene films across length scales. *Energy Environ. Sci.* **2020**, *13*, 2549–2558. [CrossRef]
19. Barsoum, M.W. *MAX Phases: Properties of Machinable Ternary Carbides and Nitrides*; John Wiley & Sons: Hoboken, NJ, USA, 2013.
20. Babar, Z.U.D.; Fatheema, J.; Arif, N.; Anwar, M.S.; Gul, S.; Iqbal, M.; Rizwan, S. Magnetic phase transition from paramagnetic in Nb 2 AlC-MAX to superconductivity-like diamagnetic in Nb 2 C-MXene: An experimental and computational analysis. *RSC Adv.* **2020**, *10*, 25669–25678. [CrossRef]

21. Fatima, M.; Fatheema, J.; Monir, N.B.; Siddique, A.H.; Khan, B.; Islam, A.; Akinwande, D.; Rizwan, S. Nb-Doped MXene With Enhanced Energy Storage Capacity and Stability. *Front. Chem.* **2020**, *8*, 168. [CrossRef]
22. Fatheema, J.; Fatima, M.; Monir, N.B.; Khan, A.S.; Rizwan, S. A comprehensive computational and experimental analysis of stable ferromagnetism in layered 2D Nb-doped Ti3C2 MXene. *Phys. E Low-Dimens. Syst. Nanostruct.* **2020**, *124*, 114253. [CrossRef]
23. Jakubowicz, J.; Sopata, M.; Adamek, G.; Siwak, P.; Kachlicki, T. Formation and Properties of the Ta-Y_2O_3, Ta-ZrO_2, and Ta-TaC Nanocomposites. *Adv. Mater. Sci. Eng.* **2018**, *2018*, 2085368. [CrossRef]
24. Naguib, M.; Gogotsi, Y. Synthesis of two-dimensional materials by selective extraction. *Acc. Chem. Res.* **2015**, *48*, 128–135. [CrossRef]
25. Naguib, M.; Tang, W.; Browning, K.L.; Veith, G.M.; Maliekkal, V.; Neurock, M.; Villa, A. Catalytic Activity of Ti-based MXenes for the Hydrogenation of Furfural. *ChemCatChem* **2020**, *12*, 5733–5742. [CrossRef]
26. Mohammadi, A.V.; Hadjikhani, A.; Shahbazmohamadi, S.; Beidaghi, M. Two-Dimensional Vanadium Carbide (MXene) as a High-Capacity Cathode Material for Rechargeable Aluminum Batteries. *ACS Nano* **2017**, *11*, 11135–11144.
27. Yoon, Y.; Tiwari, A.P.; Choi, M.; Novak, T.G.; Song, W.; Chang, H.; Zyung, T.; Lee, S.S.; Jeon, S.; An, K.-S. Precious-Metal-Free Electrocatalysts for Activation of Hydrogen Evolution with Nonmetallic Electron Donor: Chemical Composition Controllable Phosphorous Doped Vanadium Carbide MXene. *Adv. Funct. Mater.* **2019**, *29*, 1903443. [CrossRef]
28. Shan, Q.; Mu, X.; Alhabeb, M.; Shuck, C.E.; Di, P.; Zhao, X.; Chu, X.-F.; Wei, Y.; Du, F.; Chen, G. Two-dimensional vanadium carbide (V2C) MXene as electrode for supercapacitors with aqueous electrolytes. *Electrochem. Commun.* **2018**, *96*, 103–107. [CrossRef]
29. Hu, J.; Xu, B.; Ouyang, C.; Yang, S.A.; Yao, Y. Investigations on V2C and V2CX2 (X = F, OH) monolayer as a promising anode material for Li ion batteries from first-principles calculations. *J. Phys. Chem. C* **2014**, *118*, 24274–24281. [CrossRef]
30. Chen, Z.; Yang, X.; Qiao, X.; Zhang, N.; Zhang, C.; Ma, Z.; Wang, H. Lithium-Ion-Engineered Interlayers of V_2C MXene as Advanced Host for Flexible Sulfur Cathode with Enhanced Rate Performance. *J. Phys. Chem. Lett.* **2020**, *11*, 885–890. [CrossRef]
31. Lee, E.; VahidMohammadi, A.; Yoon, Y.S.; Beidaghi, M.; Kim, D.-J. Two-Dimensional Vanadium Carbide MXene for Gas Sensors with Ultrahigh Sensitivity Toward Nonpolar Gases. *ACS Sens.* **2019**, *4*, 1603–1611. [CrossRef]
32. Gao, G.; Ding, G.; Li, J.; Yao, K.; Wu, M.; Qian, M. Monolayer MXenes: Promising half-metals and spin gapless semiconductors. *Nanoscale* **2016**, *8*, 8986–8994. [CrossRef] [PubMed]
33. Blaha, P.; Schwarz, K.; Madsen, G.; Kvasnicka, D.; Luitz, J. *WIEN2k: An Augmented Plane Wave Plus Local Orbitals Program for Calculating Crystal Properties*; Vienna University of Technology, Institute of Materials Chemistry: Vienna, Austria, 2001.
34. Perdew, J.P.; Burke, K.; Ernzerhof, M. Generalized Gradient Approximation Made Simple. *Phys. Rev. Lett.* **1996**, *77*, 3865–3868. [CrossRef] [PubMed]
35. Wimmer, E.; Krakauer, H.; Weinert, M.; Freeman, A.J. Full-potential self-consistent linearized-augmented-plane-wave method for calculating the electronic structure of molecules and surfaces: O_2 molecule. *Phys. Rev. B* **1981**, *24*, 864–875. [CrossRef]
36. Dall'Agnese, Y.; Taberna, P.-L.; Gogotsi, Y.; Simon, P. Two-Dimensional Vanadium Carbide (MXene) as Positive Electrode for Sodium-Ion Capacitors. *J. Phys. Chem. Lett.* **2015**, *6*, 2305–2309. [CrossRef] [PubMed]
37. VahidMohammadi, A.; Mojtabavi, M.; Caffrey, N.M.; Wanunu, M.; Beidaghi, M. 2D MXenes: Assembling 2D MXenes into Highly Stable Pseudocapacitive Electrodes with High Power and Energy Densities. *Adv. Mater.* **2019**, *31*, 1970057. [CrossRef] [PubMed]
38. Naguib, M.; Halim, J.; Lu, J.; Cook, K.M.; Hultman, L.; Gogotsi, Y.; Barsoum, M.W. New Two-Dimensional Niobium and Vanadium Carbides as Promising Materials for Li-Ion Batteries. *J. Am. Chem. Soc.* **2013**, *135*, 15966–15969. [CrossRef] [PubMed]
39. Tang, Y.; Zhu, J.; Yang, C.; Wang, F. Enhanced supercapacitive performance of manganese oxides doped two-dimensional titanium carbide nanocomposite in alkaline electrolyte. *J. Alloy. Compd.* **2016**, *685*, 194–201. [CrossRef]
40. Feng, L.; Xuan, Z.; Zhao, H.; Bai, Y.; Guo, J.; Su, C.-W.; Chen, X. MnO_2 prepared by hydrothermal method and electrochemical performance as anode for lithium-ion battery. *Nanoscale Res. Lett.* **2014**, *9*, 290. [CrossRef]
41. Chan, Y.-L.; Pung, S.-Y.; Sreekantan, S.; Ismail, A.A. Synthesis of V_2O_5 Nanoflakes on PET Fiber as Visible-Light-Driven Photocatalysts for Degradation of RhB Dye. *J. Catal.* **2014**, *2014*, 370696. [CrossRef]
42. Halim, J.; Cook, K.M.; Naguib, M.; Eklund, P.; Gogotsi, Y.; Rosen, J.; Barsoum, M.W. X-ray photoelectron spectroscopy of select multi-layered transition metal carbides (MXenes). *Appl. Surf. Sci.* **2016**, *362*, 406–417. [CrossRef]
43. Chen, J.; Chen, K.; Tong, D.; Huang, Y.; Zhang, J.; Xue, J.; Huang, Q.; Chen, T. CO_2 and temperature dual responsive "Smart" MXene phases. *Chem. Commun.* **2015**, *51*, 314–317. [CrossRef]
44. Spanier, J.E.; Gupta, S.; Amer, M.; Barsoum, M.W. Vibrational behavior of the ${M}_{n+1}A{X}_{n}$ phases from first-order Raman scattering $(M=\mathrm{Ti},\mathrm{V},\mathrm{Cr},$ $A=\mathrm{Si},$ $X=\mathrm{C},\mathrm{N})$. *Phys. Rev. B* **2005**, *71*, 12103. [CrossRef]
45. Widjaja, E.; Sampanthar, J. The detection of laser-induced structural change of MnO_2 using in situ Raman spectroscopy combined with self-modeling curve resolution technique. *Anal. Chim. Acta* **2007**, *585*, 241–245. [CrossRef]
46. Chen, S.; Zhu, J.; Wu, X.; Han, Q.; Wang, X. Graphene Oxide−MnO_2 Nanocomposites for Supercapacitors. *ACS Nano* **2010**, *4*, 2822–2830. [CrossRef]
47. Yorulmaz, U.; Özden, A.; Perkgöz, N.K.; Ay, F.; Sevik, C. Vibrational and mechanical properties of single layer MXene structures: A first-principles investigation. *Nanotechnology* **2016**, *27*, 335702. [CrossRef]
48. Schwarz, K.; Blaha, P.; Madsen, G.K.H. Electronic structure calculations of solids using the WIEN2k package for material sciences. *Comput. Phys. Commun.* **2002**, *147*, 71–76. [CrossRef]

49. Perdew, J.P.; Yang, W.; Burke, K.; Yang, Z.; Gross, E.K.; Scheffler, M.; Scuseria, G.E.; Henderson, T.M.; Zhang, I.Y.; Ruzsinszky, A.; et al. Understanding band gaps of solids in generalized Kohn–Sham theory. *Proc. Natl. Acad. Sci. USA* **2017**, *114*, 2801–2806. [CrossRef]
50. Bowman, A.L.; Wallace, T.C.; Yarnell, J.L.; Wenzel, R.G.; Storms, E.K. The crystal structures of V_2C. *Acta Crystallogr.* **1965**, *19*, 6–9. [CrossRef]
51. Tang, Q.; Zhou, Z.; Shen, P. Are MXenes promising anode materials for Li ion batteries? Computational studies on electronic properties and Li storage capability of Ti_3C_2 and $Ti_3C_2X_2$ (X = F, OH) monolayer. *J. Am. Chem. Soc.* **2012**, *134*, 16909–16916. [CrossRef] [PubMed]
52. Naguib, M.; Mochalin, V.N.; Barsoum, M.W.; Gogotsi, Y. 25th anniversary article: MXenes: A new family of two-dimensional materials. *Adv. Mater.* **2014**, *26*, 992–1005. [CrossRef] [PubMed]
53. Zhao, S.; Kang, W.; Xue, J. MXene nanoribbons. *J. Mater. Chem. C.* **2015**, *3*, 879–888. [CrossRef]
54. Jastrzębska, A.M.; Scheibe, B.; Szuplewska, A.; Rozmysłowska-Wojciechowska, A.; Chudy, M.; Aparicio, C.; Scheibe, M.; Janica, I.; Ciesielski, A.; Otyepka, M.; et al. On the rapid in situ oxidation of two-dimensional V_2CTz MXene in culture cell media and their cytotoxicity. *Mater. Sci. Eng. C* **2021**, *119*, 111431. [CrossRef] [PubMed]
55. Kim, Y.; Gkountaras, A.; Chaix-Pluchery, O.; Gélard, I.; Coraux, J.; Chapelier, C.; Barsoum, M.W.; Ouisse, T. Elementary processes governing V 2 AlC chemical etching in HF. *RSC Adv.* **2020**, *10*, 25266–25274. [CrossRef]
56. Ravuri, S.; Kollu, P.; Jeong, S. Synthesis and properties of 2D-Titanium carbide MXene sheets towards electrochemical energy storage applications. *Ceram. Int.* **2017**. [CrossRef]